Research Article

Received: 21 August 2020 Revised: 19 October 2020 Accepted article published: 25 October 2020 Published online in Wiley Online Library: 18 November 2020

(wileyonlinelibrary.com) DOI 10.1002/pi.6149

High-fracture-toughness acrylic–polyurethane-based graft-interpenetrating polymer networks for transparent applications

Nima Alizadeh,[a,b] Mehul Barde,[a,b] Michael Minkler,[a] Asha-Dee Celestine,[c] Vinamra Agrawal,[c] Bryan Beckingham[a] and Maria L Auad[a,b]*

Abstract

Transparent materials with robust mechanical properties are essential for numerous applications and require careful manipulation of polymer chemistry. Here, polyurethane (PU) and acrylic-based copolymers out of styrene were utilized to synthesize transparent PU–acrylic graft-interpenetrating polymer networks (graft-IPNs) for the first time. In these materials, PU imparts greater flexibility, while the acrylic copolymer increases rigidity and glass transition temperature of the graft-IPNs. Kinetics of the graft-IPN synthesis was monitored using Fourier transform infrared spectroscopy and ^{1}H NMR spectroscopy through the conversion of the isocyanate group. System compatibility, degree of phase separation and material transparency were evaluated using transmission electron microscopy and UV–visible spectroscopy. Overall, higher compatibility is observed at a higher percentage of styrene in the acrylate copolymer. The thermomechanical properties of the IPNs were quantified using dynamic mechanical analysis to assess the effect of the acrylic copolymer content on fracture toughness of the resulting graft-IPNs. The high fracture toughness of the graft-IPNs, coupled with excellent transparency, demonstrates the potential of these systems for high-performance applications.

Keywords: interpenetrating polymer network (IPN); polyurethane; acrylic-based copolymers; NMR polymerization; thermomechanical; fracture toughness; viscoelastic properties

INTRODUCTION

Transparent polymeric materials with high impact resistance demonstrate good potential for a wide range of applications such as safety enclosures, aerospace applications, windshields, safety goggles and many more.[1, 2] Traditionally, glass has been used as the staple transparent material in general consumer and engineering applications.[3, 4] However, glass has high density and low impact resistance restricting its use in high-performance applications.[5] Recently, the development of transparent and high-impact-resistance polymeric materials for engineering applications has attracted widespread attention.[6] Ease of processing, low density, tunable mechanical properties, excellent impact resistance and fracture toughness of these new polymeric materials are some of the significant reasons that make them suitable candidates for advanced applications.[6, 7]

While the direct blending of polymers is one method for formulating polymers with enhanced properties,[8] the final mixing process presents challenges due to the tendency for phase separation to occur.[9, 10] To overcome phase separation between dissimilar polymers while also improving the compatibility of the solid-state material, various polymerization processes have been developed including those using graft and block copolymers and interpenetrating polymer networks (IPNs).[11]

An IPN is classified as a multi-component system where one polymer is synthesized in the presence of another.[12] Most multi-component polymeric materials form immiscible phases due to low entropy of mixing.[12] IPNs attract much attention in multi-component materials due to their physical entanglement, which brings about forced compatibility into the system, therefore increasing miscibility between the two phases.[12] Synthetic method, degree of polymerization and degree of crosslinking are factors influencing the final morphology of IPNs.[13] There are many different ways to classify IPNs based on their physical and chemical properties. A full IPN is one kind of IPN where both polymers are crosslinked, in a semi-IPN only one of the polymers is crosslinked while the other polymer is linear,[14] and in a graft-IPN both polymers are crosslinked, and a controlled amount of

* *Correspondence to: ML Auad, Department of Chemical Engineering, Auburn University, Auburn, AL 36849, USA. E-mail: auad@auburn.edu*

a *Department of Chemical Engineering, Auburn University, Auburn, AL, USA*

b *Center for Polymers and Advanced Composites, Auburn University, Auburn, AL, USA*

c *Department of Aerospace Engineering, Auburn University, Auburn, AL, USA*

bonding is allowed between the two polymers.[11, 15] A latex IPN is another kind of IPN where the IPN is in the form of latex; therefore it is a so-called interpenetrating elastomeric network.[12, 16] IPNs can also be classified as simultaneous or sequential based on the synthetic method applied. In sequential IPNs, the first polymer network is formed, swollen in the monomers of the second polymer, which is then polymerized, forming the second polymer network. In simultaneously polymerized IPNs, polymerization of the two polymer networks occurs at the same time, and no interfering reactions occur.[10, 17, 18]

Numerous groups have studied IPN systems, such as those of Millar[19] and Aylsworth and Edison,[10, 12, 20–22] who have utilized different monomers to investigate various aspects of IPNs. Extensive research on this topic has also been performed by the authors.[23, 24] In previous studies, the effects of various parameters such as curing profile, composition of the two polymer systems,[5, 7, 25–27] substitution of aliphatic and aromatic isocyanate,[25] impact of the molecular weight of diol,[7] simultaneous and sequential polymerization method[25] and using chemical bonds to synthesize graft-IPNs[28] have been studied. Overall, these studies suggested IPNs containing aliphatic isocyanate with 1400 g mol^{-1} diol and following a sequential synthetic method and with chemical bonds between the two phases presented better transparency and thermomechanical properties due to reduced phase separation from improved compatibility provided between the two phases. It was also observed that utilizing polyurethane (PU) with an acrylic copolymer, such as a poly(methyl methacrylate) (PMMA)-based copolymer, led to an improvement of ≈ 150% in fracture toughness of the acrylic copolymer. The enhancement in phase compatibility of the IPNs was also addressed.[6, 25, 28–33]

In the work reported here, the impact of varying the acrylic copolymer precursors and the chemical bonding between the two polymer networks was investigated towards the overall goal of synthesizing novel graft-IPNs with excellent compatibility, transparency and superior fracture toughness. For the first time, styrene, as one of the acrylic copolymer monomers, was utilized in the graft-IPN system. Two methods were utilized to monitor the polymerization of the two phases in the IPN systems. The compatibility of the two phases was evaluated using TEM, dynamic mechanical analysis (DMA) and UV–visible spectroscopy, while SEM and quasi-static fracture testing were used to investigate the mechanism of the fracture toughness.

EXPERIMENTAL

Materials

The PU phase was synthesized from the following compounds: 2-ethyl-2-(hydroxymethyl)-1,3-propanediol (TRIOL; 134.18 g mol^{-1}, crosslinker) purchased from Acros Organics; poly(tetramethylene ether) glycol (PTMG; ≈ 1400 g mol^{-1}) purchased from Aldrich; hexamethylene diisocyanate (DCH) purchased from TCI; and dibutyltin dilaurate (DBTDL) and triphenylbismuth (TPB) as catalysts purchased from Pfaltz & Bauer and Alfa Aesar, respectively. Ethyl acetate, purchased from Alfa Aesar, was the solvent used for the catalyst mixture. To synthesize the acrylic copolymer, styrene was purchased from Alfa Aesar, bisphenol A bis(2-hydroxy-3-methacryloxypropyl) ether (BisGMA) was purchased from Esstech and 2,2′-azobis(2-methylpropionitrile) (AIBN; thermal initiator) was purchased from Matrix Scientific. Molecular sieves (4 Å), purchased from Alfa Aesar, were used to remove the moisture from DCH, styrene, TRIOL and PTMG.

Synthesis of graft-IPNs

TRIOL (0.19 eq) and PTMG (0.12 eq) were heated to 60 °C, and the molten TRIOL and PTMG were mixed with a stirrer. Next, DCH (0.31 eq + calculated amount of DCH to react with BisGMA) was added to the mixture, and the mixture was stirred. The PU phase accounted for 25 wt% of the final composition for all specimens.

For the second phase, various amounts of BisGMA were dissolved into styrene, and then AIBN (1 wt% of total co-monomer mass) was dissolved into the mixture. Then PU monomers and acrylic-phase monomers were mixed. Amounts of 600 µL of DBTDL per 50 g of PU (0.02 mol L^{-1} ethyl acetate solution) and 600 µL of TPB (0.001 mol L^{-1} ethyl acetate solution) were added to the monomer mixture at the end of this stage for the poly-addition polymerization of the PU phase. Finally, the mixture was cured in closed aluminium molds for 24 h at 40 °C, followed by 24 h at 60 °C and finally 24 h at 80 °C.

Figure 1 shows the poly-addition polymerization chemistry of the PU network. Simple schematics of the reaction occurring for acrylic copolymer synthesis and IPN structure are shown in Figs 2 and 3, respectively.

Characterization

Fourier transform infrared (FTIR) spectroscopy was performed with a Nicolet 6700 FTIR spectrometer from Thermo Scientific (USA) in attenuated total reflection IR mode. FTIR experiments

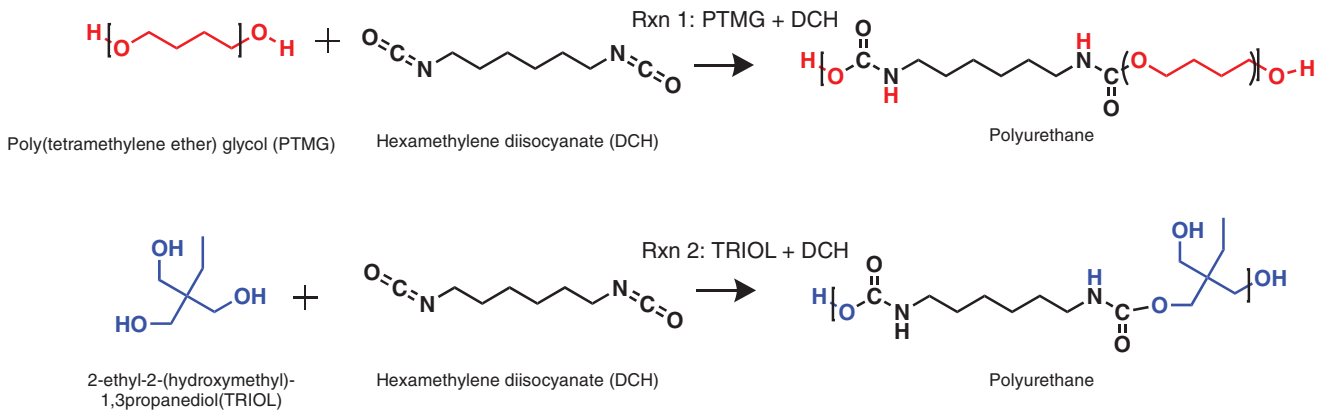

Figure 1. Two poly-addition polymerization reactions that form the PU phase. Top: reaction between PTMG and DCH; bottom: reaction between TRIOL and DCH.

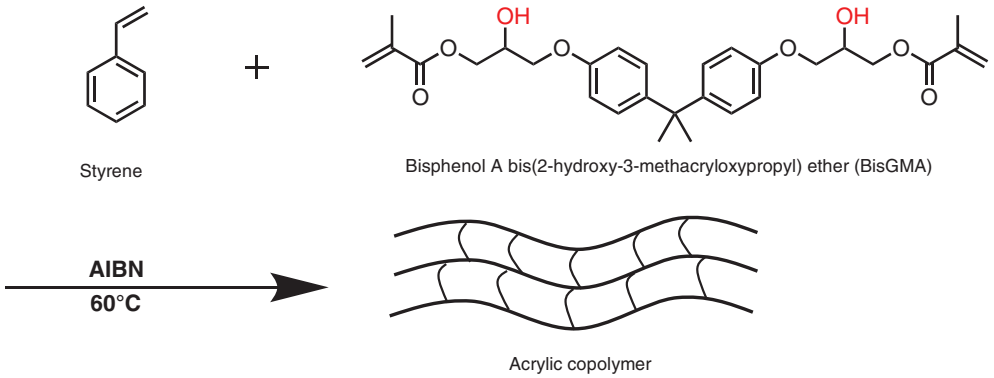

Figure 2. Free radical polymerization of acrylic copolymer from styrene and BisGMA.

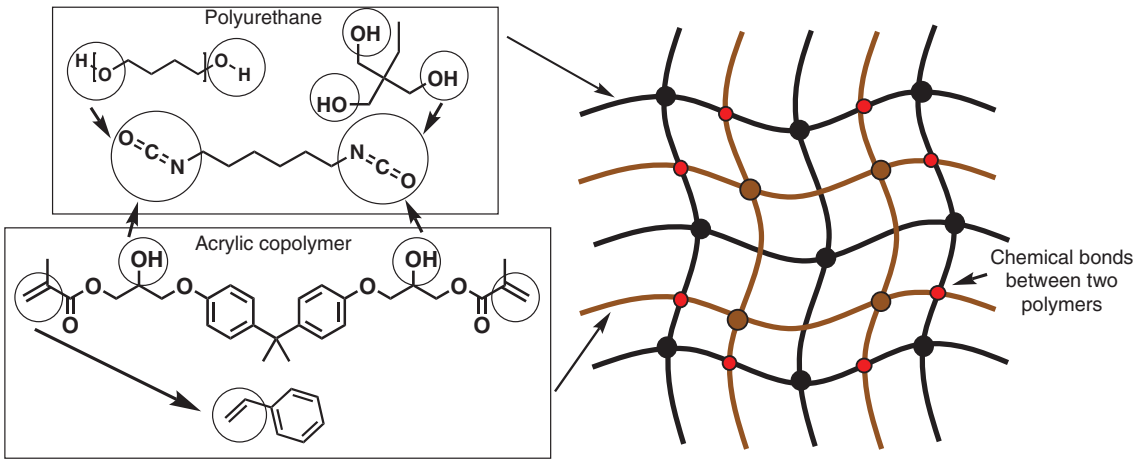

Figure 3. Simple schematic of IPN network structure.

were performed from 400 to 4000 cm^{-1} with 64 scans and using a resolution of 4 cm^{-1}.

Low-field ^1H NMR spectroscopy was performed on an Oxford Pulsar 60 MHz (1.4 T) NMR spectrometer using Wilmad class B eight-inch high-throughput tubes (5 mm outer diameter, 4 mm internal diameter). The ^1H NMR experiment was conducted as an arrayed experiment in Oxford Spin Flow software with 64 scans per run, a recycle delay of 2 s and a spectral width of 50 000 Hz. This combination of parameters yielded an approximate sampling time of 5 min and 48 s per spectrum. The spectra were analyzed using Mnova software.

A Zeiss EVO 50 variable-pressure SEM instrument with digital imaging and EDS (with the IPNs sputter-coated with an EMS 550X auto sputter coating device with carbon coating attachment) was used to study the surface morphology of the specimens. The specimens were immersed in liquid nitrogen, broken and the fracture events visualized using SEM. A Zeiss EM 10C 10CR TEM instrument was used to examine the interior morphology of the samples. Samples were stained using a 2.5% aqueous solution of osmium tetroxide (OsO_4) for one week, as reported by Kato[34] prior to microtoming. A Cary 60 UV–visible spectrometer from Agilent (USA) was used to verify the transparency of the samples (250–800 nm wavelength).

A TA Instruments RSA 3 dynamic mechanical analyzer was used for studying the thermomechanical properties of the IPNs. Flexural testing was performed from 25 to 200 °C with a sinusoidal strain amplitude of 0.1% and 0.1 Hz frequency, and a heating rate of 5 °C min^{-1}.

The fracture toughness properties of specimens were characterized using quasi-static fracture testing performed with a three-point bending condition following ASTM D5045.[35] Equations (1)–(3) were used to calculate the plane-strain fracture toughness K_{Ic}, where a is crack length, W is specimen width, B is specimen thickness and $0 < x < 1$:

$$K_{Ic} = \left(\frac{P_Q}{BW^{1/2}}\right) f(x) \tag{1}$$

$$f(x) = 6x^{1/2}\,\frac{1.99 - x(1-x)(2.15 - 3.93x + 2.7x^2)}{(1+2x)(1-x)^{3/2}} \tag{2}$$

$$x = \frac{a}{W} \tag{3}$$

Cured specimens were cut to bars with dimensions of 55 mm × 12 mm × 3 mm using a Boss laser (LS 3655). An edge notch 4 mm in length was cut into the samples with a saw, and the edge tip subsequently sharpened with a razor blade. Single edge notched bend testing was performed on the specimens using an Instron 5565 with 1 kN static load cell. The load and displacement data were recorded up to crack initiation and during

stable crack growth. The load at crack initiation (P) was used to calculate K_{Ic}. MATLAB was utilized to calculate K_{Ic} with Eqns (1)–(3), and at least five specimens were tested for each composition.[31]

RESULTS AND DISCUSSION

Analysis of isocyanate conversion using FTIR measurements

The compositions (using a 10 g sample basis) of synthesized materials investigated with FTIR and NMR spectroscopies and their corresponding nomenclature are presented in Table 1. The isocyanate (NCO) conversion was studied using FTIR spectroscopy. The measurement is based on the decay in intensity of the peak assigned to isocyanate absorption during polymerization. The absorption peak of the isocyanate group is assigned to approximately 2270 cm^{-1}. The C—H stretch absorption band at 2850–3000 cm^{-1} was used as an internal standard due to the constant strength of this band during the reaction.[36] The isocyanate conversion was calculated using Eqn (4)[37]:

$$p = 1 - \frac{A_{NCO}/A_{CH_2}}{(A_{NCO}/A_{CH_2})_0} \quad (4)$$

where p is the isocyanate conversion, A_{NCO} is the integrated absorbance for the isocyanate group, A_{CH_2} is the integrated absorbance for the C—H stretch band and $(A_{NCO}/A_{CH_2})_0$ is the relative absorbance extrapolated to time zero.

FTIR spectra for PU-PT at 0, 18, 36 and 64 min and at three days are shown in Fig. 4, where the isocyanate absorption peak (2270 cm^{-1}) decreases during polymerization while the C—H stretch absorption peak (2800–3000 cm^{-1}) remains constant. This indicates the isocyanate groups react with the hydroxyl groups of the TRIOL and PTMG to form the PU network as expected.

The isocyanate conversion *versus* time data extracted from the FTIR spectra are shown in Fig. 5. While initial polymerization rates across the series are similar (except for PU-B), PU-P is the first to reach near completion. PU-B clearly shows the slowest polymerization rate, likely due to the secondary hydroxyl groups in BisGMA and the corresponding steric hindrance compared to the PTMG primary hydroxyl groups.[38] PU-PTB shows a higher polymerization rate in comparison to PU-PT due to the presence of BisGMA which provides more hydroxyl groups into the system. PU-PT and IPN80/20 follow the same trend due to the dominant behavior of PU in isocyanate conversion and the steric effect of acrylic copolymer in the IPN system.

FTIR spectroscopy was also utilized for pure acrylic copolymer with 20 wt% BisGMA and 80 wt% styrene (COP80/20) to characterize the free radical polymerization at 60 °C, which forms the second polymer network in IPN80/20. Samples were cured for 24 h at 60 °C and then cured for 24 h at 80 °C and their FTIR spectra obtained at the beginning of the synthesis and after two days of curing (Fig. 6). Peaks at 774 and 908 cm^{-1} corresponding to the out-of-plane bending of ═C—H and at 1600–1660 cm^{-1} corresponding to C═C can be used to track polymerization. Both of these peaks decrease during free radical polymerization due to the consumption of double bonds. Moreover, a peak corresponding to sp^3 C—H stretching appears after two days of curing in the range 2850–3000 cm^{-1} as additional confirmation of consumption of C═C—H to form sp^3 C—H.

Analysis of isocyanate conversion via low-field NMR spectroscopy

Reaction progress for PU-P and PU-PT was also tracked using an Oxford Instruments Pulsar 60 MHz NMR spectrometer. Briefly, an initial spectrum of PTMG was collected prior to the addition of DCH and two drops of each catalyst, DBTDL and TPB, dissolved in ethyl acetate. The reaction mixture was agitated via stirring with copper wire and manual shaking of the tube before being placed into the probe bore. The spectrometer was tuned and matched to the sample, and then an arrayed experiment was commenced. Note that the lag time (time from the addition of the catalyst to the start of the NMR spectroscopy tracking experiment) was accounted for in both the reaction progress diagram (Fig. 7) and the subsequent data analysis.

Tetramethylsilane (a standard additive used to align most 1D ^1H NMR spectra) was not used here to eliminate any possible interactions with the reaction media. Instead, all spectra were shifted based on the far-right peak attributed to the PTMG backbone of PU-P (1.56 ppm).[36] This peak also served as an internal calibration standard as the underlying protons associated with this peak (for both systems) are conserved; for the PU-PT system, the TRIOL aliphatic arm also contributes to this peak, so five additional protons are accounted for as shown in Fig. 8.

Unfortunately, due to the spectral overlap in the aliphatic region of the NMR spectra (Fig. 7), the consumption of hydroxyl groups could not be tracked directly. However, in both cases, the formation of urethane linkages can be traced through the formation of N—H protons. By utilizing this method, we combine the advantages of more traditional DSC reaction tracking through heat evolution and that of the FTIR spectroscopy through bond identity, as discussed in this paper. Furthermore, as has been discussed elsewhere, an additional advantage of the low-field NMR spectrometer used here is the soft-lock algorithm, which eliminates the need for deuterated solvents and allows for examination of protons without any adulteration of the reaction media.[39]

Table 1. Prepared sample compositions used for FTIR and NMR spectroscopy

	Polyurethane 25 wt%			Acrylic copolymer 75 wt%	
Sample	PTMG (wt%)	TRIOL (wt%)	DCH (wt%)	Styrene (wt%)	BisGMA (wt%)
PU-PT	70.8	7.2	22	—	—
PU-P	89	—	11	—	—
PU-B	—	—	24.7	—	75.3
PU-PTB	14.2	1.4	24.2	—	60.2
IPN80/20	16.9	1.7	9.9	57.2	14.3
COP80/20	—	—	—	80	20

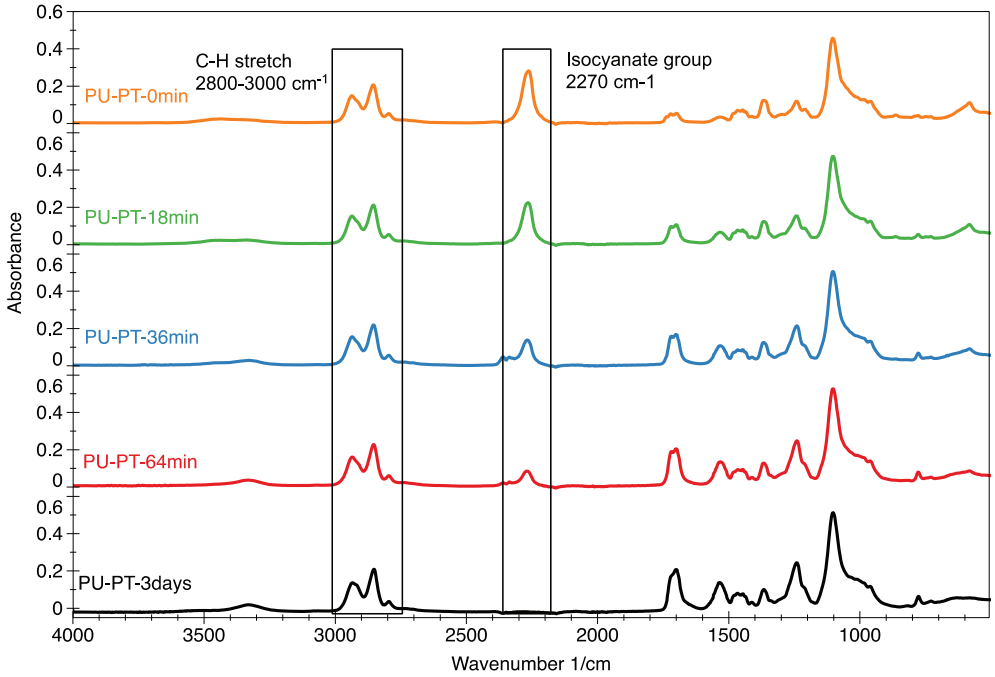

Figure 4. FTIR spectra of PU-PT sample at five different times.

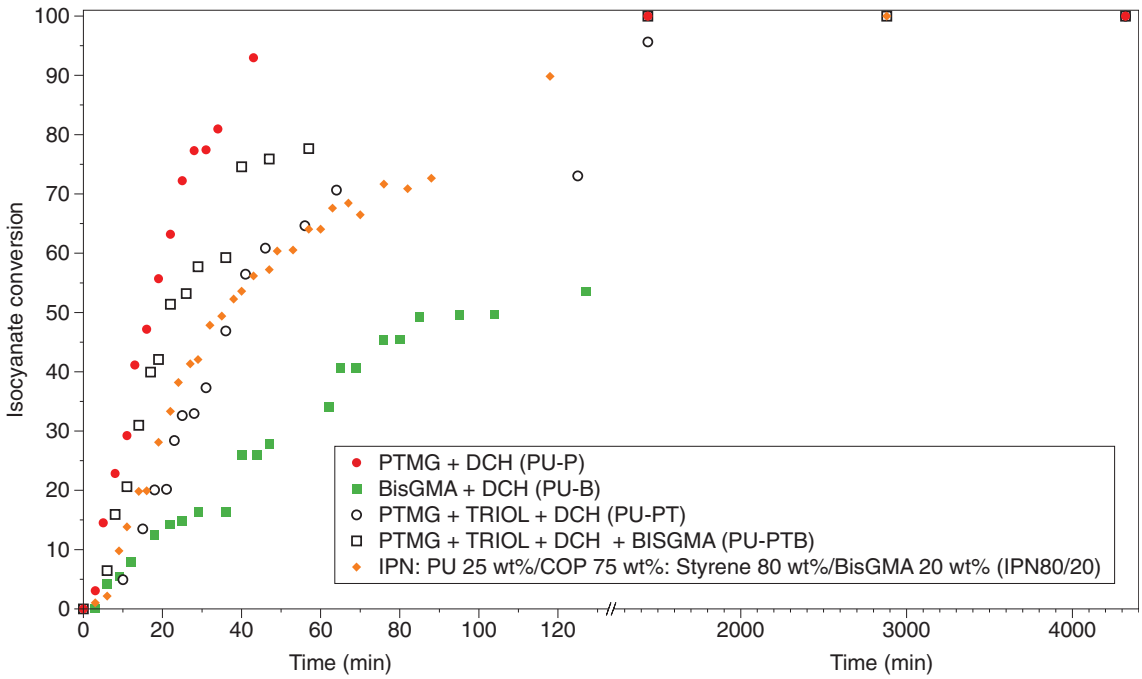

Figure 5. Isocyanate conversion of various samples.

As shown in Fig. 7, the peak at 5.94 ppm grows in intensity over time due to the continuous formation of secondary amine peaks as urethane linkages are formed. In the case of PU-P, each urethane linkage is strictly from the consumption of —OH groups on the PTMG chain ends. However, for PU-PT this metric of conversion is complicated by the presence of additional hydroxyl groups on the arms of TRIOL. Nonetheless, the overall conversion to isocyanate linkages was tracked as a function of peak area and number of protons via Eqn (5):

$$\text{Conversion}\,(\%) = 100 \times \frac{A_{5.94} N_{1.56}}{A_{1.56} N_{5.94}} \tag{5}$$

where A_i is the peak area at i ppm and N_j is the number of protons associated with the peak at j ppm. Peak areas (A_i) were extracted from Gaussian fits to the peaks after spectral shifting, automatic phasing and automatic baselining in Mnova software. For PU-P, $N_{1.56}$ = 76.665 and $N_{5.94}$ = 2.0157; for PU-PT, $N_{1.56}$ = 81.70375 and $N_{5.94}$ = 6.04704. These values are calculated for each

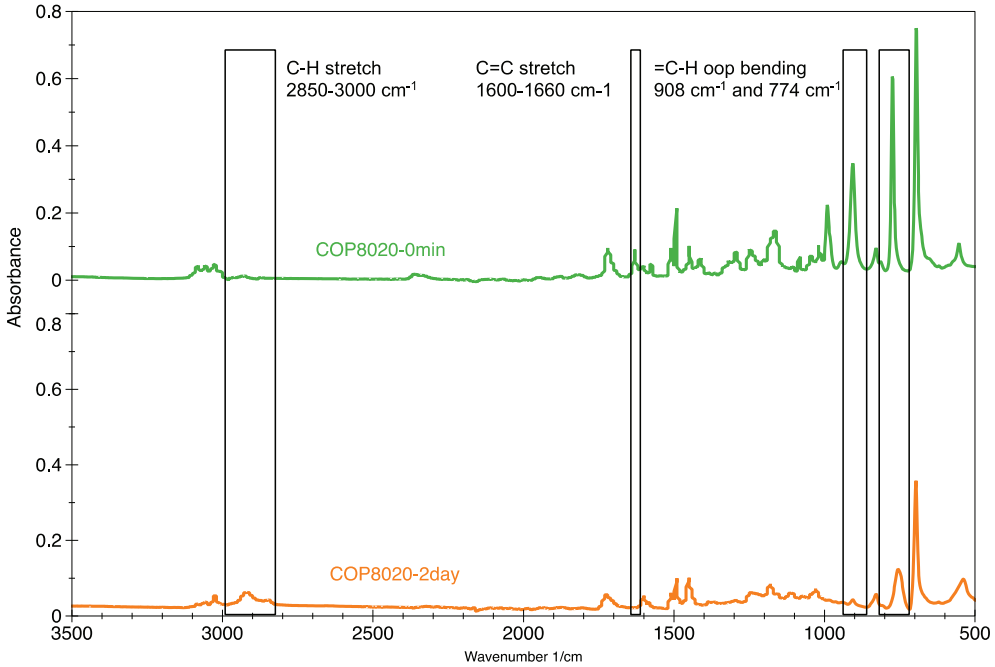

Figure 6. FTIR spectra of acrylic copolymer at 0 min (top) and after two days of curing (bottom). (oop, out-of-plane.)

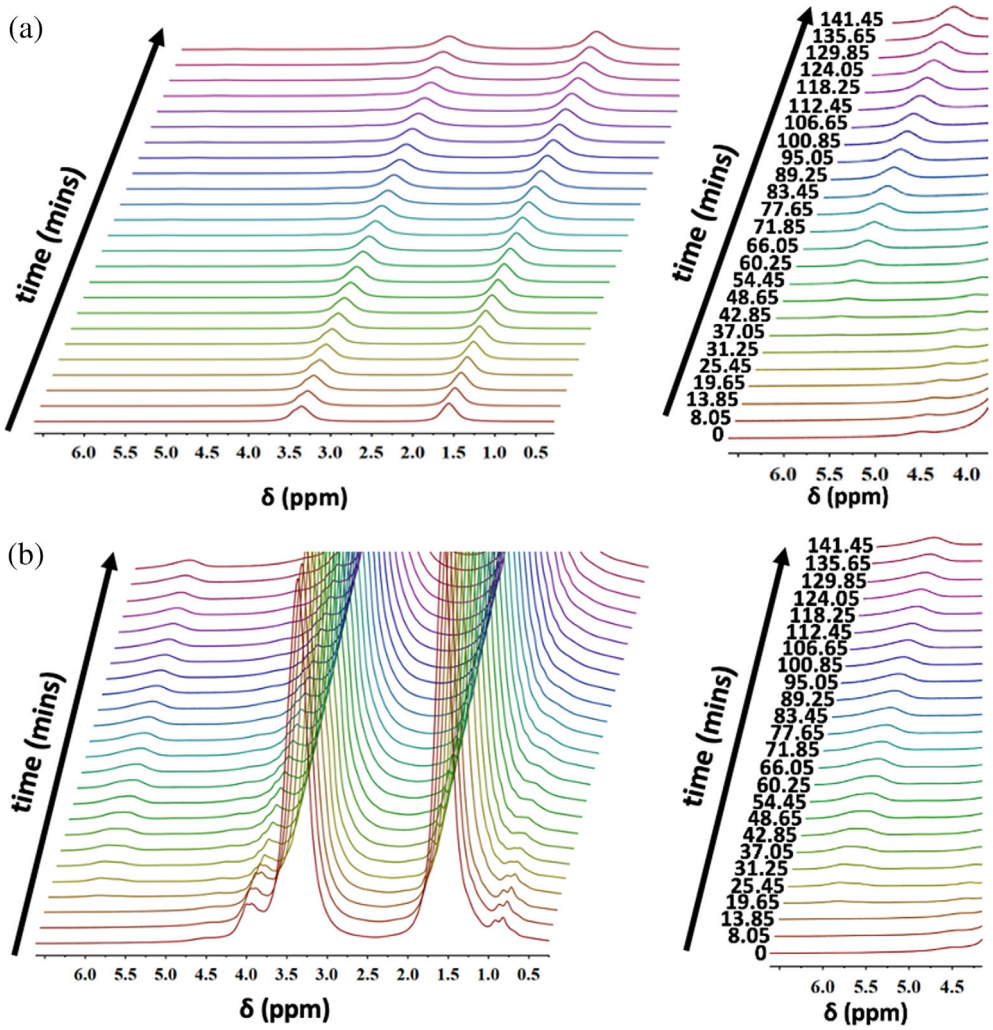

Figure 7. Left: NMR spectra from *in situ* reaction monitoring of (a) PU-P and (b) PU-PT with (right) spectra enlarged to show PU linkage peak.

chemistry from the reaction stoichiometry and chemical structures shown in Fig. 8.

In the case of PU-P, this analysis assumes only one DCH molecule is present in the 'repeat unit' of the network, while PU-PT has the potential for up to three DCH molecules; two amine protons and six amine protons, respectively. This is important as the network is complicated by the availability of hydroxyl groups from these two different mer units. Extracted conversion *versus* time data and their comparison with FTIR data are shown in Fig. 9.

As shown in Fig. 9, both systems exhibit a lag time at the beginning of the reaction in the NMR instrument, which we attribute to the low reaction rate at room temperature as the reaction medium approaches the spectrometer operating temperature of 37 °C. However, the reaction can be effectively tracked over time as the DCH is incorporated within the polymeric structure, and isocyanate groups are converted into secondary amines within the urethane linkages. While the data points appear to be non-continuous, it is essential to note that the spectrometer is averaging the signal over 64 scans that are acquired over a cycle time of approximately 5 min and 48 s; i.e. the resulting isocyanate conversion is time-averaged. Additionally, the conversion in each case reaches a maximum at approximately the same time as extracted from FTIR spectroscopy after accounting for the thermal lag time. Overall, we find this method to provide adequate and facile means to track both reaction progress and specific bond formation.

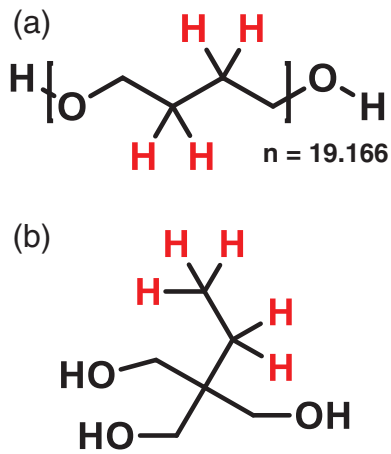

Figure 8. Protons used in the calculation of $N_{1.56}$ are highlighted in red for (a) PTMG and (b) TRIOL.

Network morphology

A series of IPNs with different styrene to BisGMA content in the acrylic network were synthesized, and their morphology examined with TEM (Fig. 10). The lines observed in Figs 10(a)–(c) are tool marks produced during the microtoming procedure. The pure acrylic copolymer (Fig. 10(a)) shows a homogeneous dispersion of the polymeric component throughout the copolymer sample and is utilized as the control experiment for comparisons. No clear OsO_4-stained domains are observed in this sample. In the IPN samples, the PU regions become black after sample staining, while the acrylic phase does not interact with OsO_4 and remains clear. Figures 10(b)–(d) display TEM images of IPNs with 70, 80 and 90 wt% of styrene, respectively. In Fig. 10(b), a distinct black domain is observed in the sample due to the incompatibility of the two polymers containing 70 wt% styrene. However, the IPN composed of 80 wt% styrene shows a fine dispersion of the two polymers with no well-defined domains in the image. As described by Bird *et al.*, the absence of defined domain shapes indicates a good interpenetration of two phases.[25] The finest phase domains of the samples, as observed by TEM, typically indicate the highest level of interpenetration between the two polymers.[30] Figure 10(d) corresponds to the IPN system with 90 wt% styrene and demonstrates good interpenetration between the two polymers with less phase separation in comparison to the

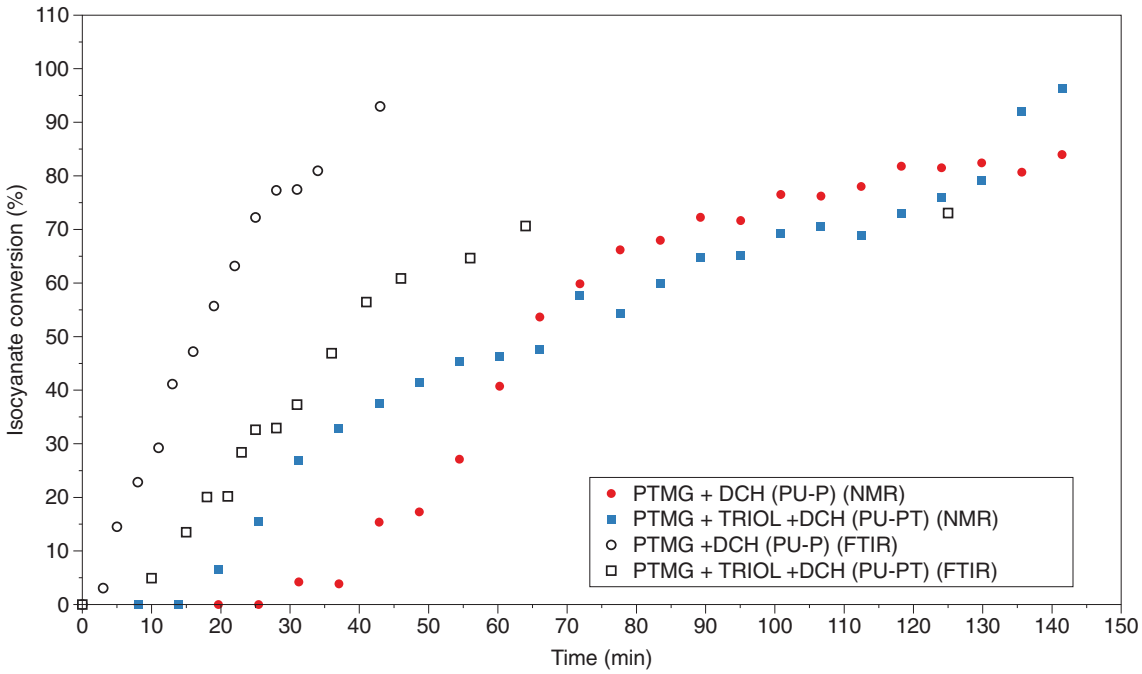

Figure 9. Reaction progress for both systems as a function of isocyanate conversion.

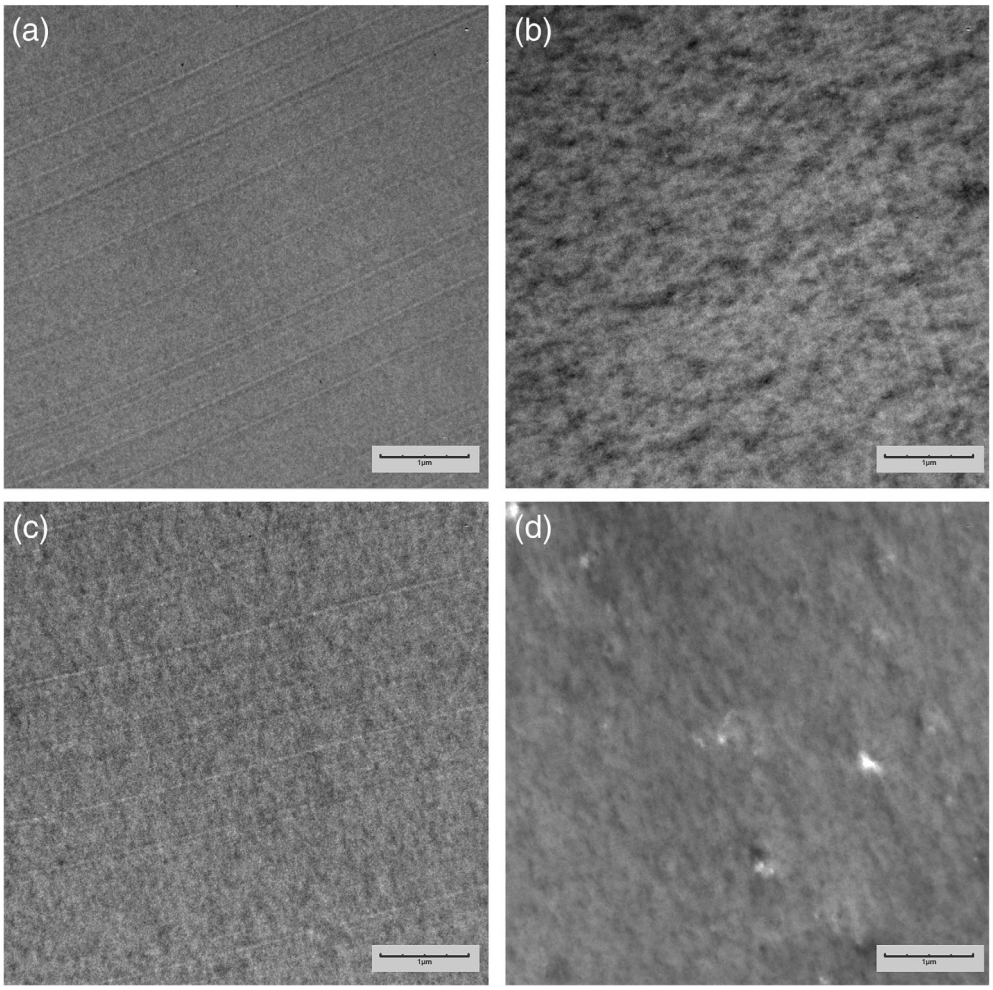

Figure 10. TEM images of (a) copolymer: styrene 80 wt%/BisGMA 20 wt%; IPN samples with 25 wt% PU and 75 wt% acrylic copolymer with various acrylic copolymer precursors: (b) styrene 70 wt%/BisGMA 30 wt%; (c) styrene 80wt%/BisGMA 20 wt%; (d) styrene 90 wt%/BisGMA 10 wt%.

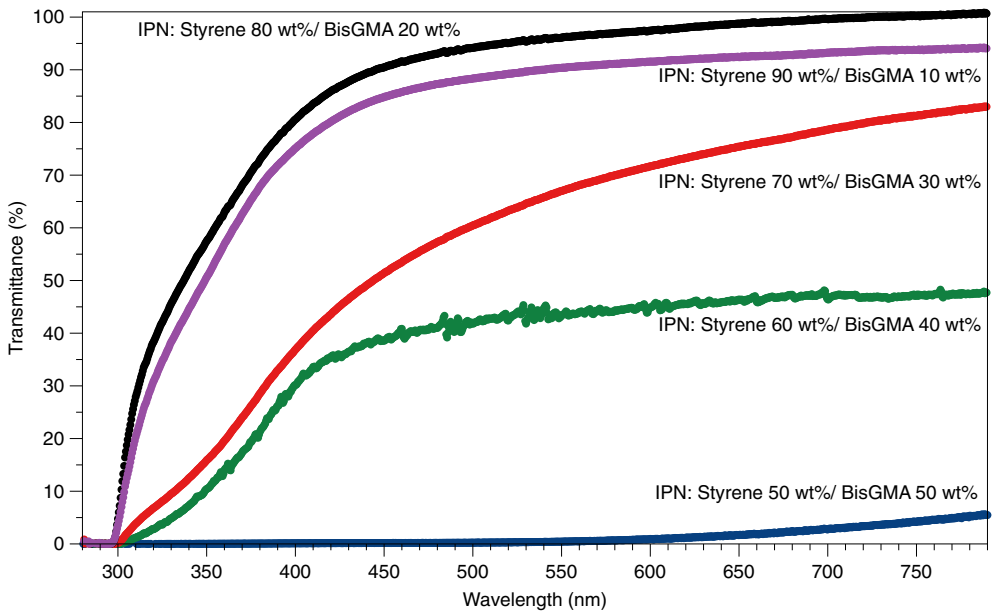

Figure 11. UV–visible spectra of IPNs with 25 wt% PU and 75 wt% acrylic copolymer with different copolymer composition.

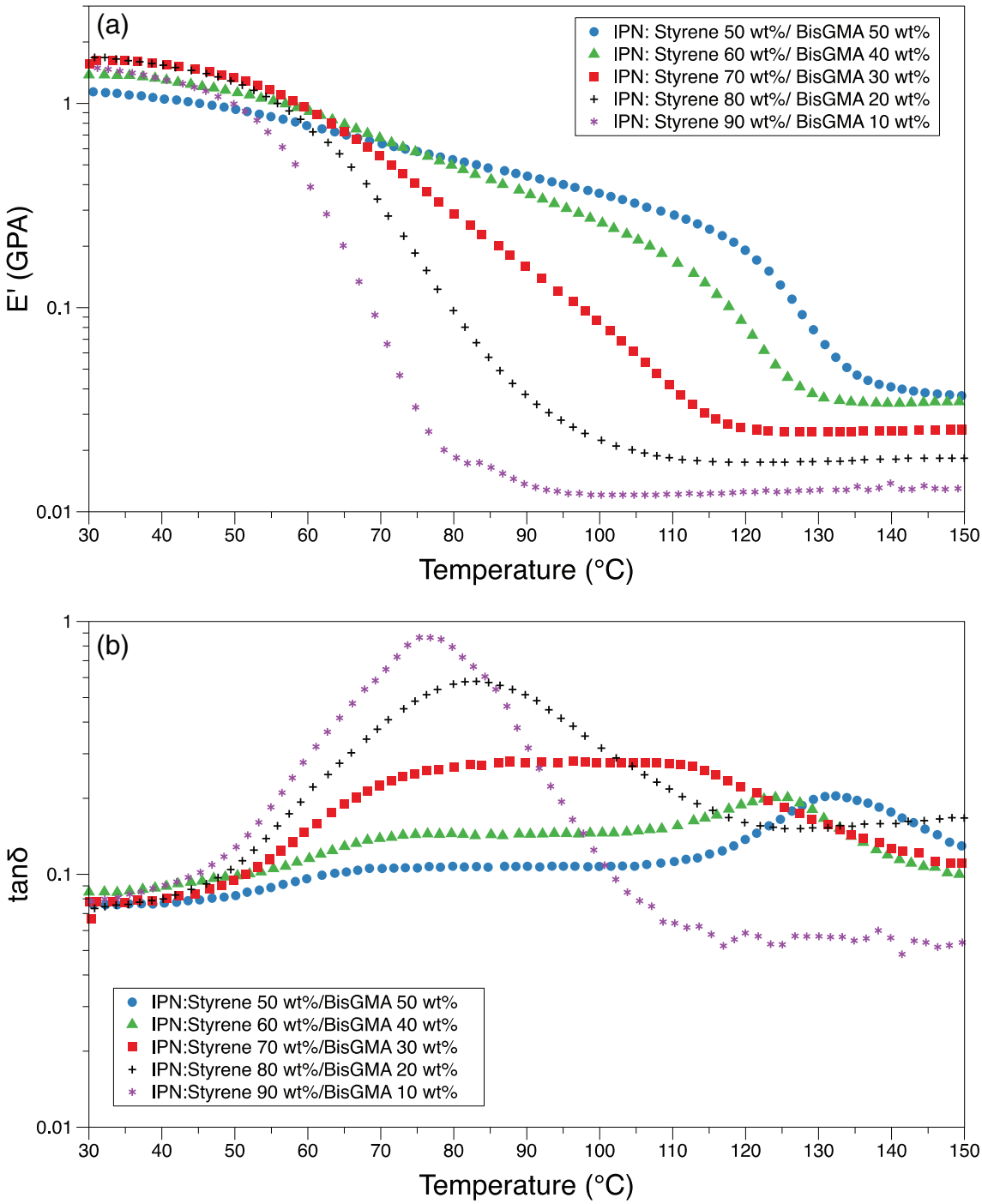

Figure 12. Flexural test results: (a) storage modulus *versus* temperature and (b) tan δ *versus* temperature for IPNs with 25 wt% PU and 75 wt% acrylic copolymer with various acrylic copolymer precursors.

sample with 70 wt% of styrene. The smaller size and thereby higher mobility of styrene in comparison to BisGMA within the PU network likely improve swelling of the forming PU network and decrease phase separation.

It was also observed that utilizing a linear isocyanate (such as DCH) has a positive effect on the compatibility of two phases.[25] Ballestero *et al.* also used TEM to study the impact of post-curing processes on domain size and interpenetration of PU with PMMA and observed better dispersion between the two polymers after post-curing due to the additional chemical bonds formed between the two polymer networks during this process.[28]

Degree of transparency

IPN transparency was investigated using UV–visible spectrophotometry with the results for the IPNs of various styrene to BisGMA compositions shown in Fig. 11. Transparency is a strong function of composition as samples with 50 wt% styrene show almost no transparency while increasing styrene content leads to increasing

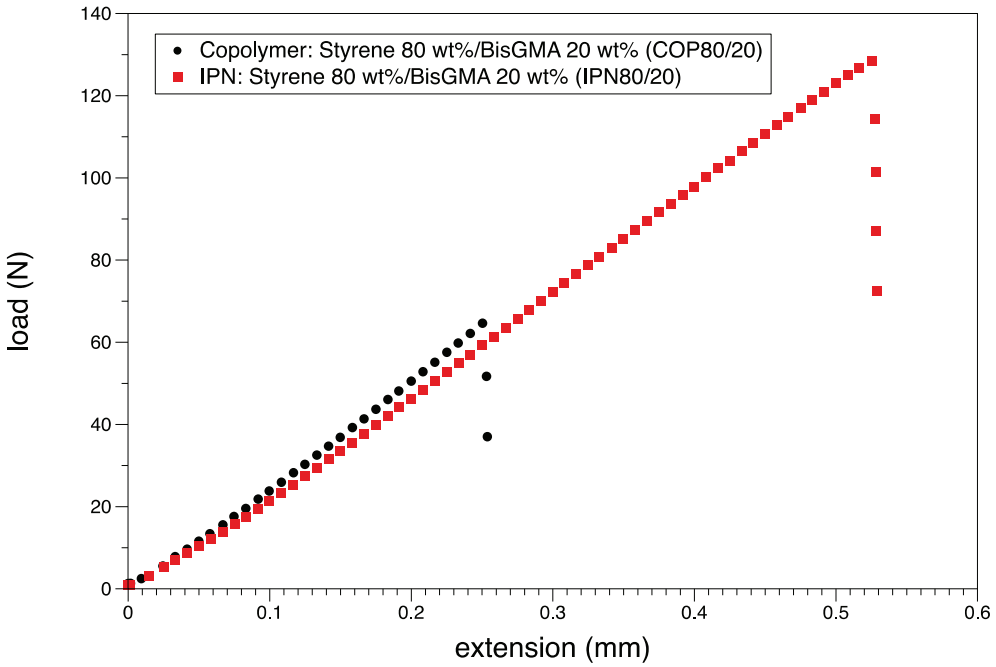

Figure 13. Representative load–displacement plots for acrylic copolymer and IPN with 25 wt% PU and 75 wt% acrylic copolymer.

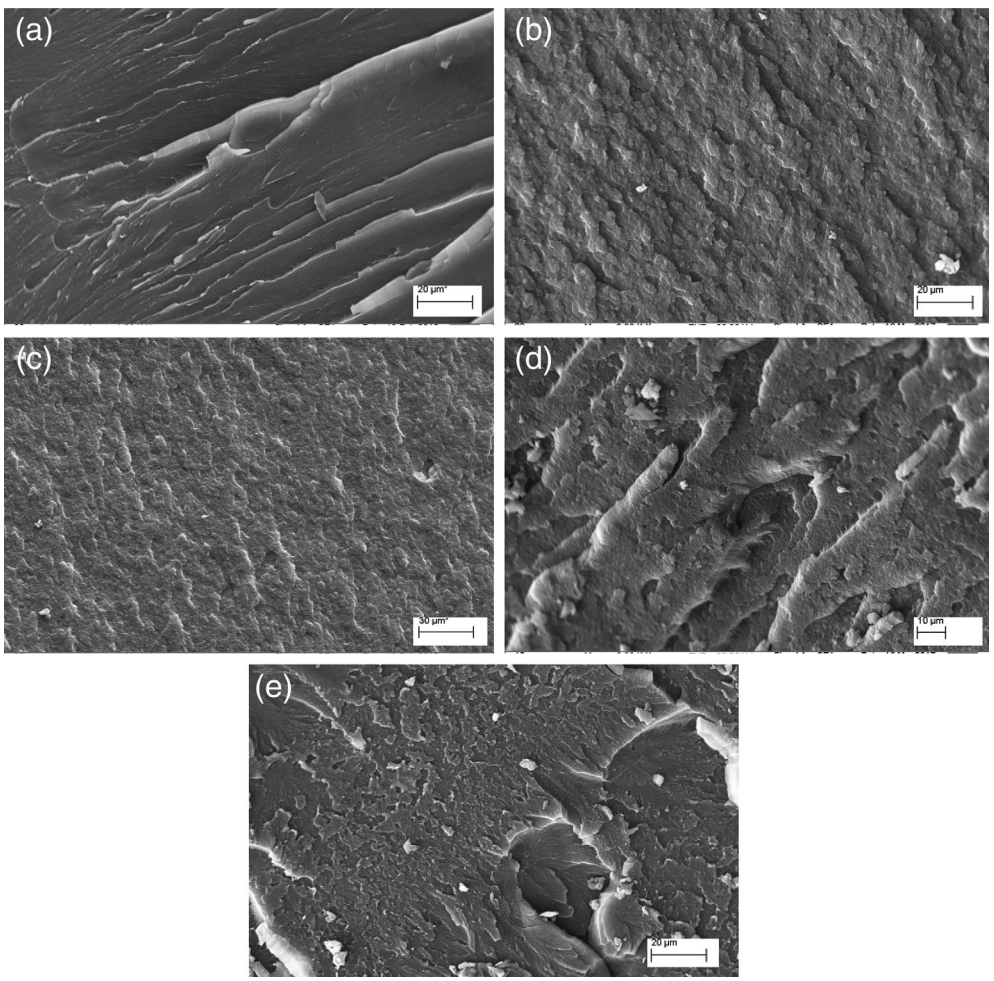

Figure 14. SEM images: (a) copolymer: styrene 80 wt%/BisGMA 20 wt%; IPN samples with 25 wt% PU and 75 wt% acrylic copolymer with various acrylic copolymer precursors: (b) styrene 50 wt%/BisGMA 50 wt%; (c) styrene 60 wt%/BisGMA 40 wt%; (d) styrene 70 wt%/BisGMA 30 wt%; (e) styrene 80 wt %/BisGMA 20 wt%.

transparency. For IPN samples with 80 wt% styrene (Fig. 10(c)) and 90 wt% styrene (Fig. 10(d)), the domain sizes are below 380 nm on average; for these samples, good transparency was observed. In the case of IPN sample with 70 wt% styrene (Fig. 10(b)), it shows the domain in the range of the light wavelength, and the transmittance is considerably reduced. Ultimately, samples with 80 and 90 wt% of styrene show transmittance values close to 100% in the visible wavelength region, indicating good compatibility between the phases.

Thermomechanical characterization

Thermomechanical properties of the synthesized IPNs were evaluated using DMA. Figure 12(a) shows the storage modulus of the samples *versus* temperature; samples with a higher percentage of styrene show higher initial moduli due to better compatibility between the two phases. Figure 12(b) shows the tan δ results of the samples *versus* temperature. The 50 wt% styrene IPN shows two peaks in tan δ, indicating the presence of two glass transition temperatures, and is an indication of phase separation between the PU and acrylic copolymer constituents. The gap between the two peaks decreases with increasing styrene content, due to the greater compatibility between the two phases. The 70 wt% styrene IPN (Fig. 12(b)) exhibits a flat peak in tan δ, due to improved compatibility but the remaining presence of phase separation. The IPN with 80 wt% of styrene shows only one peak in its tan δ curve, demonstrating better compatibility between the two IPN constituents as observed with TEM and UV–visible spectroscopy. The peak becomes sharper for the 90 wt% styrene IPN sample, further verifying enhanced phase compatibility. Broader peaks in samples with a lower percentage of styrene suggest that there are several relaxation mechanisms involved in the systems, which are more heterogeneous at the microscopic scale.[25, 28, 40]

Fracture properties

Fracture toughness of the copolymer with 80 wt% styrene and 20 wt% BisGMA (COP80/20) and the IPN with 75 wt% copolymer (80 wt% styrene) and 25 wt% PU (IPN80/20) were characterized, and a representative load *versus* displacement plot is shown in Fig. 13. Both samples show a linear elastic response up to the peak load, followed by brittle failure. IPN80/20 exhibited a higher load capacity at failure indicating enhanced fracture toughness and higher extension before brittle failure in comparison to the neat acrylic copolymer. Plane-strain fracture toughness K_{Ic} of COP80/20 and IPN80/20 was 1.61 ± 0.16 and 2.2 ± 0.19 MPa $m^{1/2}$, respectively. IPN80/20 shows approximately 40% improvement in fracture toughness in comparison to COP80/20 as the presence of PU in the system improves the fracture properties by providing additional flexibility. Moreover, IPN80/20 shows more than 100% improvement in fracture toughness in contrast to virgin atactic polystyrene with fracture toughness of 1.00 ± 0.20 MPa $m^{1/2}$ and PMMA with fracture toughness of 1.08 ± 0.18 MPa $m^{1/2}$.[41,42]

SEM was used to investigate the fracture mechanism of the synthesized IPNs with various acrylic network compositions. The SEM images of the fractured samples are shown in Fig. 14. With increasing styrene content, an observable decrease in the roughness and surface area is observed, corresponding to less energy dissipation during fracture propagation. Although increasing the percentage of styrene increases the compatibility between the two phases, it decreases the fracture toughness of the samples. Similar behavior has been reported in the literature, where obtaining a rougher surface enhances the fracture toughness properties of samples.[20, 43]

CONCLUSIONS

Acrylic–PU-based graft-IPNs were synthesized, and their reaction kinetics and thermomechanical and optical properties investigated. Chemical bonding between the two polymers was utilized to increase the interpenetration between the two polymer networks. FTIR spectroscopy revealed complete isocyanate conversion and the formation of PU linkages and chemical bonds between the two polymer networks. ^{1}H NMR spectroscopy was also utilized to track the kinetics of PU formation, and the results were found to be in good agreement with those from FTIR spectroscopy.

The interplay of IPN composition and related material properties was investigated as a function of IPN styrene content. Incorporation of the acrylic copolymer network provided higher rigidity and better thermomechanical properties to the material. In contrast, higher flexibility was imparted by the PU phase, increasing the impact resistant and the fracture toughness of the IPNs. DMA, TEM and UV–visible spectrophotometry results indicate that increasing the percentage of styrene in the system improves the interpenetration between the two polymer networks and therefore enhances the compatibility between them. SEM images suggest that increasing the styrene content decreases fracture toughness as observed from the change in surface roughness upon fracture. Significant improvement was observed in fracture toughness of graft-IPNs in comparison to an acrylic copolymer in graft-IPNs. Such graft-IPNs with excellent transparency and fracture toughness better than those of polystyrene and PMMA have considerable potential in high-fracture-toughness applications.

ACKNOWLEDGEMENT

The authors thank NSF-CREST Center for Sustainable Lightweight Materials (C-SLAM) award no. 1735971 for funding this study.

REFERENCES

1 Parimal JP, Gary AG, Peter GD, James WM, editors. Transparent ceramics for armor and EM window applications. ProcSPIE. (2000).
2 Kobayashi A and Ohtani N, Dynamic fracture in aerospace high polymers, in *Resins for Aerospace*, Vol. **132**. American Chemical Society, pp. 367–377 (1980).
3 Martin AMAG, *Glass: A World History*. University of Chicago Press, Chicago, IL (2002).
4 Rawson H, *Properties and Applications of Glass*. Elsevier Scientific Publishing, (1980).
5 Jajam KC, Bird SA, Auad ML and Tippur HV, *Polym Test* **32**:889–900 (2013). https://doi.org/10.1016/j.polymertesting.2013.04.010.
6 Méndez RB, *Sequential Graft-Interpenetrating Polymer Networks Based on Polyurethane and Acrylic/Ester Copolymers*. Auburn University, Auburn, AL (2015).
7 Sundaram BM, Mendez RB, Auad ML and Tippur HV, *Polym Test* **70**: 348–362 (2018). https://doi.org/10.1016/j.polymertesting.2018.06.032.
8 Robeson LM, *Polymer Blends: A Comprehensive Review*. Hanser, (2007).
9 Panapitiya NP, Wijenayake SN, Huang Y, Bushdiecker D, Nguyen D, Ratanawanate C *et al.*, *Polymer* **55**:2028–2034 (2014). https://doi.org/10.1016/j.polymer.2014.03.008.
10 Sperling LH and Mishra V, *Polym Adv Technol* **7**:197–208 (1996). https://doi.org/10.1002/(Sici)1099-1581(199604)7:4<197::Aid-Pat514>3.0.Co;2–4.

11 Sperling LH, Klempner D and Utracki LA, *Interpenetrating Polymer Networks*. American Chemical Society, Washington, DC (1994).
12 Dave VJ and Patel HS, *J Saudi Chem Soc* **21**:18–24 (2017). https://doi.org/10.1016/j.jscs.2013.08.001.
13 Sheu HR, El-Aasser MS and Vanderhoff JW, *J Polym Sci A: Polym Chem* **28**:629–651 (1990). https://doi.org/10.1002/pola.1990.080280314.
14 Pissis P, Georgoussis G, Bershtein VA, Neagu E and Fainleib AM, *J Non-Cryst Solids* **305**:150–158 (2002). https://doi.org/10.1016/S0022-3093(02)01091-8.
15 Sperling LH, *Interpenetrating Polymer Networks and Related Materials*, Vol. **12**. Plenum Press, New York (1981).
16 Sperling LH, *J Polym Sci Macromol Rev* **12**:141–180 (1977). https://doi.org/10.1002/pol.1977.230120103.
17 Sperling LH, Interpenetrating polymer networks: an overview, in *Interpenetrating Polymer Networks*, Vol. **239**. American Chemical Society, pp. 3–38 (1994).
18 Mita I and Akiyama S, Molecular design of network polymers, in *Macromolecular Design of Polymeric Materials*. Marcel Dekker, New York, p. 400 (1997).
19 Millar JR, *J Chem Soc*:1311–1317 (1960). https://doi.org/10.1039/JR9600001311.
20 Chen CH, Chen WJ, Chen MH and Li YM, *Polymer* **41**:7961–7967 (2000). https://doi.org/10.1016/S0032-3861(00)00173-7.
21 Fan LH, Hu CP and Ying SK, *Polymer* **37**:975–981 (1996). https://doi.org/10.1016/0032-3861(96)87280-6.
22 Sundararajan S, Samui AB and Kulkarni PS, *Sol Energy Mater Sol Cells* **149**:266–274 (2016). https://doi.org/10.1016/j.solmat.2015.12.040.
23 Sibaja B, Matheus CP, Mendez RB, Vega-Baudrit JR and Auad ML, *J Renewable Mater* **5**:231–240 (2017). https://doi.org/10.7569/JRM.2017.634113.
24 Sibaja B, Matheus CP, Mendez RB, Farag R, Baudrit JRV and Auad ML, *J Renewable Mater* **5**:241–250 (2017). https://doi.org/10.7569/JRM.2017.634114.
25 Bird SA, Clary D, Jajam KC, Tippur HV and Auad ML, *Polym Eng Sci* **53**:716–723 (2013). https://doi.org/10.1002/pen.23305.
26 Jajam KC, Tippur HV, Bird SA and Auad ML, Dynamic fracture and impact energy absorption characteristics of PMMA-PU transparent interpenetrating polymer networks (IPNs), in *Dynamic Behavior of Materials*, Vol. **1**, ed. by Song B, Casem D and Kimberley J. Springer International, Cham, pp. 277–284 (2014).
27 Jajam KC, Bird SA, Auad ML and Tippur HV, Development and characterization of PU-PMMA transparent interpenetrating polymer networks (t-IPNs), in *Dynamic Behavior of Materials*, Vol. **1**, ed. by Proulx T. Springer, New York, pp. 117–121 (2011).
28 Ballestero R, Sundaram BM, Tippur HV and Auad ML, *Express Polym Lett* **10**:204–215 (2016). https://doi.org/10.3144/expresspolymlett.2016.19.
29 Hillerström A, Andersson M, Pedersen JS, Altskär A, Langton M, van Stam J *et al*., *J Appl Polym Sci* **114**:1828–1839 (2009). https://doi.org/10.1002/app.30673.
30 Qin C-L, Cai W-M, Cai J, Tang D-Y, Zhang J-S and Qin M, *Mater Chem Phys* **85**:402–409 (2004). https://doi.org/10.1016/j.matchemphys.2004.01.019.
31 Alizadeh N, Bird SA, Mendez RB, Jajam KC, Alexander AC, Tippur HV *et al*., Synthesis and characterization of high performance interpenetrating polymer networks with polyurethane and poly(methyl methacrylate), in *Unsaturated Polyester Resins*. Elsevier, pp. 243–255 (2019).
32 Bird SA, *Interpenetrating Polymer Networks with Polyurethane and Methacrylate-based Polymers*. Auburn University, Auburn, AL (2013).
33 Huang J and Zhang L, *Polymer* **43**:2287–2294 (2002). https://doi.org/10.1016/S0032-3861(02)00028-9.
34 Kato K, *J Polym Sci B: Polym Lett* **4**:35–38 (1966). https://doi.org/10.1002/pol.1966.110040107.
35 Standard Test Methods for Plane-Strain Fracture Toughness and Strain Energy Release Rate of Plastic Materials.
36 Pavia DL, Lampman GM and Kriz GS, *Introduction to Spectroscopy*, 3rd edn. Thomson Learning, Washington (2001).
37 Cateto CA, Barreiro MF and Rodrigues AE, *Ind Crops Prod* **27**:168–174 (2008). https://doi.org/10.1016/j.indcrop.2007.07.018.
38 Anslyn EV, Dougherty DA and Sausalito CUS, *Modern Physical Organic Chemistry*. University Science Books, Sausalito, CA (2006).
39 Chakrapani SB, Minkler MJ and Beckingham BS, *Analyst* **144**:1679–1686 (2019). https://doi.org/10.1039/C8AN01810C.
40 Auad ML, Aranguren M and Borrajo J, *J Appl Polym Sci* **66**:1059–1066 (1997). https://doi.org/10.1002/(SICI)1097-4628(19971107)66:6<1059::AID-APP6>3.0.CO;2-H.
41 Serrano A, Welsch G and Gibala R, *Polym Eng Sci* **22**:946–949 (1982).
42 Choi SR and Salem JA, *J Mater Res* **8**:3210–3217 (1993). https://doi.org/10.1557/JMR.1993.3210.
43 Hsieh KH, Han JL, Yu CT and Fu SC, *Polymer* **42**:2491–2500 (2001). https://doi.org/10.1016/S0032-3861(00)00641-8.

